A Driving-behavior-based SoC Prediction Method for Light Urban Vehicles Powered by Supercapacitors

Houlian Wang, Gongbo Zhou, *Member, IEEE,* Rui Xue, Yuanjie Lu, Julie A McCann

***Abstract*—Range anxiety is one of the problems that hinders the large-scale application of electric vehicles (EVs). We propose a driving-behavior-based State of Charge (SoC) prediction (DBSP) algorithm to overcome this problem. This algorithm can determine whether drivers can reach their destinations while also predicting the SoC if drivers were to return the trip. First, two supercapacitor equivalent circuit models are established, with one based on the historical average power and the other based on the equivalent current, which is proposed in this algorithm. Then, based on the equivalent transformation of the two models, an analytical expression relating the historical average power and the predicted SoC is derived by using the equivalent current as a 'bridge'. Therefore, the predicted SoC can be dynamically adjusted in response to recorded historical data, including the output power, speed and distance of EVs powered by supercapacitors. The simulation results demonstrate that the total prediction error is less than 0.5% of the real SoC at different initial SoC and temperature, which represents idealized behavior-based driving. In contrast, in actual driving experiments, the total prediction error is less than 3% of the real SoC at different initial SoC and temperature.**

***Index Terms*—SoC prediction; driving behavior; equivalent current; electric vehicles; supercapacitor**

I. Introduction

Supercapacitors, or electronic double-layer capacitors, have high power densities, long lifespans, and high efficiency and can respond quickly when charging or discharging. In contrast, traditional batteries need a longer charge times, which has restrained the development of battery based vehicles. Because of these beneficial characteristics, supercapacitors have been used in urban electric vehicles (EVs). For example, supercapacitor buses [1], light rail vehicles [2].

For the passenger vehicles, there has been some literature discussing the possibility of supercapacitor-based EVs [3]. Light EVs are designed in [4] with full pure supercapacitors and the EV performances of acceleration and travelled distance are predicted and valuated. A small EV prototype is built to research the feasibility of using supercapacitor based EVs in the public transport of Mexico City, validated in simulation and experiments [5]. A sightseeing car powered by supercapacitors is designed and analyzed in [6], which may also be used in city tourism.

From application requirements, because of faster charging and longer life time than batteries, supercapacitors are indeed a competitive candidate for EVs with the specified applications. Sunvault Energy has cooperated with Edison Power to produce a graphene supercapacitor powered fully electric vehicle, the Edison Electron One [7]. Another potential application is supercapacitor-based electric taxis. For battery powered electric taxis, it takes at least 30 minutes to reach 80% power even with the latest charging technology [8]. The time cost of charging these cabs in a station will directly reduce taxi drivers' incomes. Supercapacitors overcome this time wastage since it takes just a few minutes to charge fully. The travel range for supercapacitor vehicles is also not a problem, because for example cabs would mainly travel in urban areas, which can be equipped with charging stations throughout a city.

However, all EVs are, and will remain for the foreseeable future, characterized by a considerably smaller range than that of conventional vehicles. Hence, drivers usually worry about whether they can arrive at destinations or whether they need to find a charging station first. Consequently, 'range anxiety' is unavoidable and is an impediment to the development of electric vehicles [9]. Therefore, it is important to judge whether an EV can arrive at its destination and to know the remaining charge when it reaches it.

In fact, many models have been built to evaluate the states of supercapacitors, which makes it possible to solve the aforementioned problem. For instance, the simplest supercapacitor circuit model is the Rint model, which includes an ideal capacitor and a resistor [10]. Based on this model, more detailed models have been proposed. The RC parallel branch model has a different time constant in each RC branch, which can reflect the internal charge distribution process very well [11]. RC series-parallel branch models are also proposed, including the Thevenin model, DP model and 3-RC model [12]. In addition, the RC transmission line model has been developed based on Porous Electrode Theory, with consideration of both dynamic and long-time behaviors [13].

Methods for tackling range anxiety have also been developed.

This work was supported in part by the National Natural Science Foundation of China (No. 51575513), Jiangsu Provincial Natural Science Foundation of China (No. BK20180033), and A Project Funded by the Priority Academic Program Development of Jiangsu Higher Education Institutions (PAPD).

H. Wang, G. Zhou, R. Xue, Y. Lu are with School of Mechanical and Electrical Engineering, China University of Mining & Technology, Xuzhou 221116, China (whl@cumt.edu.cn, gbzhou@cumt.edu.cn, 15395014900@163.com, TS18050120P31@cumt.edu.cn).

J. McCan is with School of Computing, Imperial College London, London SW7 2AZ, UK (j.mccann@imperial.ac.uk).

One strategy is range prediction. The driving range is predicted based on various constant-speed trips and the initial state of charge [14]. To reduce the uncertainties of predictive range, Enthaler proposed a method that utilizes history-based average energy consumption and remaining energy [15]. An efficient approach was introduced to compute probabilistic attainability maps for electric vehicles [16]. However, range prediction can only help drivers understand whether they can reach the destination, but it fails to provide quantitative information: telling the users the remaining capacity which provides confidence and keeps them in the loop. Another strategy is runtime prediction. A remaining dischargeable time prediction framework is presented based on accurate battery modeling and state estimation [17]. The runtime is forecasted based on the estimated state of energy in the batteries [18]. Although useful to some extent, runtime prediction cannot offer exact qualitative information: telling drivers whether they can reach the end, or quantitative information: informing users of the remaining capacity.

State of charge (SoC) prediction is a promising strategy, as it provides both qualitative as well as quantitative information. This strategy is advantageous because SoC is defined as the percentage of remaining capacity relative to the maximum capacity of a supercapacitor and is thus an indicator of the residual capacity of a supercapacitor, and also because range anxiety would be alleviated greatly if an EV driver knows the future SoC before starting the car. For instance, the information allows the driver to understand whether he or she can complete the entire journey so that they can judge whether they need to find a charger, where an EV is not fully charged. In addition, if a driver knows the remaining SoC in the future when the driver reaches the destination, they can drive with relatively less stress. Although an accurate prediction of the SoC is crucial for EV onboard applications, to the best of the authors' knowledge, no studies have focused on SoC prediction techniques, which is a relatively newer field of study compared with SoC estimation [19, 20], State of Health (SOH) determination [21, 22] and State of Power (SOP) prediction [23].

Therefore, an SoC prediction method based on driving behavior is proposed in this paper. This method uses the historical average output power of EVs to represent average output power for the next trip. Then, the future average output power is transferred into a new concept, equivalent current, which is first proposed in this paper. Next, travel time is predicted according to historical speed and distance. Finally, the future SoC at the destination is predicted based on the equivalent current and predicted travel time, if drivers were to return the trip.

The contributions of this paper are as follows.

1. A SoC prediction method based on driving behavior is novel to this paper.

2. The virtual concept of equivalent current is the first proposed to simplify the prediction process.

3. A mathematical expression is first established between SoC and average power of a supercapacitor, using the definition of SoC by current.

The remainder of this paper is divided into the following sections. In section II, two equivalent circuits of a supercapacitor are built, including an equivalent circuit of a supercapacitor under constant power discharge and an equivalent circuit of a supercapacitor under constant current discharge. In section III, the derivation of the SoC prediction method is explained. Section IV presents parameter identification results. Section V presents the simulation results in an idealized situation with invariable driving behavior in each simulation at different temperature. Section VI presents the experimental results at different temperature for a practical case of a driver driving a real vehicle. Section VII presents the conclusions of this paper.

II. MODELING

Two equivalent circuit models are introduced in this section. One model simulates the supercapacitor under constant power loading, representing the average output power of the supercapacitor during a trip. The other model considers the supercapacitor under constant current discharge, representing equivalent current for SoC prediction.

A. Constant Power Discharge Modeling

Definition 1: Historical average power is defined as $P_{ha}=(P_{h1}+P_{h2}+...+P_{hn})/n$, where P_{h1} is the practical average power in the first trip; P_{h2} is the practical average power in the second trip; P_{hn} is the practical average power in the nth trip; and n is the number of trips.

We use a constant power load, average power, to replace the practical external load for a trip in the modeling since the energy consumed by the practical external load is equal to the energy consumed by the average power. The energy consumed by the practical external load varies, and is difficult to model. In contrast, the average power out of supercapacitors remains roughly unchanged for each trip, making it easy to calculate, although practical output power differs from trip to trip. Therefore, historical average power in Definition 1 is nearly equal to average output power for a future trip, which is normally constant. Hence, constant power loading, i.e. historical average power, is modeled to represent average output power for a future trip in the following model.

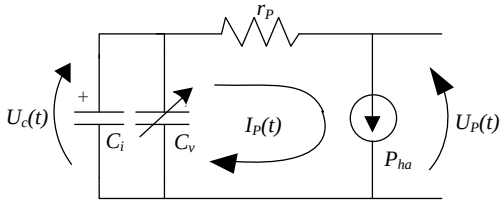

Fig. 1. Equivalent circuit of the supercapacitor under constant power loading

Model 1: The supercapacitor is modeled using the Rint equivalent circuit model with a linear capacitor [24, 25]. The model comprises a constant internal resistance r_P and a linear capacitor, which is composed of a constant capacitor C_i and a voltage-dependent capacitor, $C_v=KU_c(t)$. The linear double-layer capacitance has an initial potential U_{co} and an

applied constant discharge power loading, P_{ha} , which is predicted from the historical record or the parameters of electric vehicles. The internal potential $U_c(t)$, terminal potential $U_P(t)$ and current during discharge $I_P(t)$ are all functions of time.

B. Constant Current Discharge Modeling

Definition 2: Equivalent current is defined as $I_e = (1/T) \times \sum_{j=1}^{n} i_j t_j \eta_j$, where $T = \sum_{j}^{n} t_j$. i_1 is the practical discharge current for a duration t_1 with Coulombic efficiency η_1 for a trip; i_2 is the practical discharge current for a duration t_2 with Coulombic efficiency η_2 for the trip; i_n is the practical discharge current for duration t_n with Coulombic efficiency η_n for the trip.

It is better to obtain the real-time current for the next trip, if a prediction of future SoC is needed. In this case, the SoC can be achieved by using the ampere-hour method. In reality, it is extremely difficult to obtain the future current exactly. We propose a virtual concept, i.e., equivalent current, to replace the complex accumulated items to overcome this problem. In fact, equivalent current is constant for a trip according to Definition 2. Therefore, it is easy and simple to use the product of equivalent current and equivalent discharge time to replace the cumulative sum of actual real-time current, actual discharge time and actual Coulombic efficiency. This means that the SoC can be predicted if the equivalent current and equivalent discharge time can be ascertained.

The equivalent current is represented by the constant current in model 2. This model is established to reflect equivalent current, so it is not a real supercapacitor model. The equivalent current can be achieved by establishing a relationship between itself (the constant current in model 2) and average output power (the constant power in model 1) according to the principle of conservation of energy. The equivalent discharge time can be estimated based on traveling distance and speed. The greatest benefit of this concept is that the practical discharge current does not need to be calculated.

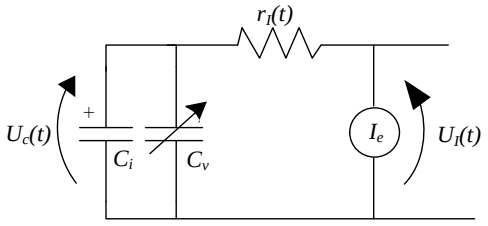

Fig. 2. The equivalent circuit of a supercapacitor under constant current discharge

Model 2: The equivalent circuit of the supercapacitor under constant current discharge is shown in Fig. 2. The constant capacitor C_i, voltage-dependent capacitor C_v, initial potential U_{co} and internal potential $U_c(t)$ are the same as those in Fig. 1. A constant discharge current loading (equivalent current I_e) is applied in this model. The internal potential U_c(t) , terminal potential $U_I(t)$ and internal resistance $r_I(t)$ are functions of time. r_P in Fig. 1 is the practical internal resistance and can be measured, whereas $r_I(t)$ in Fig. 2 is the virtual resistance and must be calculated.

III. SoC Prediction Algorithm

In this section, the SoC prediction algorithm is formulated based on the model of constant power discharge (representing average output power) and the model of constant current discharge (representing equivalent current). Based on the two models, we first use the historical average power estimating the average output power for the future trip to derive the equivalent current according to the principle of conservation of energy. Then, the equivalent current is used as the 'bridge' between historical average power and the future SoC. The predicted SoC is calculated by using the equivalent current instead of the practical discharge current.

Before derivation, we first give some basic definitions based on the linear supercapacitor model, which is different from constant capacitance model. The definition of capacitance is borrowed from [26], which is suitable in both models.

$$C = C_i + KU_c = \frac{dQ}{dU_c} \tag{1}$$

The second one is the relationship among the current, internal potential and linear capacitance.

$$I_P(t) = \frac{dQ}{dt} = \frac{CdU_c}{dt} = (C_i + KU_c)\frac{dU_c}{dt} \tag{2}$$

Now, the derivation is as follows. The first step is to transform the historical average power in model 1 into the equivalent current in model 2 by analytic derivation.

To begin with, the relationship between the two models needs to be expressed using equal equations. Historical average power is given information from historical data recorded in an EV. To complete the transformation from constant power into constant current, we must make sure the energy consumed in both models is identical. Namely, the energy expended by the internal resistance (formula (3)) and the energy consumed by the external load (formula (4)) in both models are equal.

$$W_{r_P} = W_{r_I} \tag{3}$$

$$W_P = W_I \tag{4}$$

W_{r_P} is energy consumed by the internal resistance r_P in model 1. W_{r_I} is energy consumed by the internal resistance $r_I(t)$ in model 2. W_P is energy consumed by the constant discharge power loading P_{ha} in model 1. W_I is the energy consumed by the constant discharge current loading I_e . Formula (3) can then be represented by g and can be rewritten as formula (5) by integration.

$$g = \int_0^t I_P(\tau)^2 r_P d\tau = \int_0^t I_e^2 r_I(\tau) d\tau \tag{5}$$

where *t* is the discharge time. The current $I_P(t)$ is time-varying, and the internal resistance r_P is constant in the equivalent circuit under constant power loading in Fig. 1. In contrast, the

current I_e is constant and the internal resistance $r_I(t)$ is time-varying in the equivalent circuit under constant current discharge in Fig. 2.

Furthermore, formula (4) can be presented in detail. In model 1, the energy consumed under constant power loading W_P can be obtained as

$$W_P = P_{ha} t \tag{6}$$

In model 2, because the terminal potential $U_I(t)$ is time-varying, the energy consumed by the constant current load W_I can also be obtained by integration:

$$W_I = \int_0^t U_I(\tau) I_e d\tau \tag{7}$$

where the terminal potential $U_I(t)$ is

$$U_I(t) = U_c(t) - I_e r_I(t) \tag{8}$$

The internal potential U_c(t) is not known, and we have to build a relationship to represent U_c(t) with other known elements. The following derivation can be achieved.

$$Q_0 - Q_t = I_e \times t \tag{9}$$

Hence, the equation (10) can be changed as the following

$$\int_0^{U_{c0}} C dU_c - \int_0^{U_c(t)} C dU_c = I_e \times t \tag{10}.$$

We can get U_c(t) by solving the aforementioned formulas (8-10)

$$U_c(t) = \frac{-C_i + \sqrt{C_i^2 - 2KI_e t + K^2 U_{c0}^2 + 2KC_i U_{c0}}}{K} \tag{11}.$$

Substituting formula (11) and (8) into (7) yields

$$W_I = \int_0^t U_c(t) I_e d\tau - \int_0^t I_e^2 r_I(\tau) d\tau \tag{12}.$$

The first item can be calculated

$$\int_0^t U_c(t) I_e d\tau = -\frac{C_i I_e}{K} t - \frac{1}{3K^2}[(a - 2KI_e t)^{3/2} - a^{3/2}] \tag{13}$$

where

$$a = C_i^2 + K^2 U_{c0}^2 + 2KC_i U_{c0} \tag{14}.$$

Substituting formulas (7) and (13) into (5), we obtain

$$P_{ha} t = -\frac{C_i I_e}{K} t - I_e^2[(a - 2KI_e t)^{3/2} - a^{3/2}] - \int_0^t I_e^2 r_I(\tau) d\tau \tag{15}.$$

Finally, the equivalent current can be obtained using formulas (3) and (10):

$$\begin{aligned} I_e = 3\Bigg[& (-\frac{b}{6} - \frac{1}{3}a^{\frac{3}{2}} - \frac{1}{4}C_i^3 + \frac{1}{2}C_i a + K^2(P_{ha} t + g)) \\ & \times (2b + 4a^{\frac{3}{2}} + C_i^3 - 6C_i a + (-12P_{ha} t - 12g)K^2)^{\frac{1}{3}} \\ & + (-\frac{1}{4}C_i^2 + \frac{a}{3})(2b + 4a^{\frac{3}{2}} + C_i^3 - 6C_i a + (-12P_{ha} t - 12g)K^2)^{\frac{2}{3}} \\ & + 2C_i(-\frac{b}{6} - \frac{1}{3}a^{\frac{3}{2}} - \frac{1}{8}C_i^3 + \frac{1}{2}C_i a + K^2(P_{ha} t + g)) \Bigg] \\ & / \Bigg[2Kt(2b + 4a^{\frac{3}{2}} + C_i^3 - 6C_i a + (-12P_{ha} t - 12g)K^2)^{\frac{2}{3}} \Bigg] \end{aligned} \tag{16}$$

where

$$b = \sqrt{((-24P_{ha}\,t - 24g)K^2 + 2C_i^3)a^{\frac{3}{2}} - 12a^{\frac{5}{2}}C_i + 36(P_{ha}t + g)^2 K^4 + (-6C_i^2 + 36a)(P_{ha} + g)C_i K^2 - 3C_i^4 a + 9C_i^2 a^2 + 4a^3} \tag{17}.$$

And also, we use $g = \int_0^t I_P(\tau)^2 r_p d\tau$ to replace the last item, because of formula (5). The current $I_p(t)$ of the supercapacitor under constant power loading can be obtained from formulas (18) and (19), and the derivation is provided in Appendix.

$$\begin{aligned} t = & \frac{C_i}{4P}\Bigg\{\Bigg[U_c(U_c + \sqrt{U_c^2 + 4r_p P_{ha}}) + 4r_p P \ln(U_c + \sqrt{U_c^2 + 4r_p P_{ha}})\Bigg] \\ & + \frac{K}{6P}\Bigg[U_c^3 + (U_c^2 + 4r_p P)^{\frac{3}{2}}\Bigg]\Bigg\}_U^{U_{c0}} \end{aligned} \tag{18}$$

$$I_P(t) = -(C_i + KU_c(t)) \quad \& \quad U_c(t) = \frac{U_c - \sqrt{U_c^2 + 4r_p P_{ha}}}{2r_p} \tag{19}$$

The next step is to predict the SoC by using the obtained equivalent current. The SoC is typically calculated using the following formula based on the ampere-hour method, if practical current, discharge time and Coulombic efficiency are known

$$SoC = SoC_0 - \frac{\sum_{j=1}^{n} i_j t_j \eta_j}{Q_{\max}},$$

where $Q_{\max}$ is the maximum available capacity of the supercapacitor. In this paper, we can use $\sum_{j=1}^{n} i_j t_j \eta_j = I_e T$ in Definition 2 to calculate the SoC; thus, we have

$$SoC = SoC_0 - \frac{I_e T}{Q_{\max}}$$

The discharge time can be calculated by the ratio of the historical average distance traveled S to the historical average speed V during a trip; then, we have

$$SoC = SoC_0 - \frac{I_e (S/V)}{Q_{\max}} \tag{20}$$

The procedure for implementing the SoC prediction algorithm is as follows.

DBSP Algorithm

1: Initialize the historical average power P_{ha}, historical average distance S, historical average speed V, initial state of charge SoC_0, internal potential U_{c0} and internal resistance r_P
2: Determine the time step Δt
3: for $t = 1 : \Delta t : (S/V)$
4: Calculate the current $I_p(t)$ of the supercapacitor under constant power loading according to formula (18) and (19)
5: end
6: Calculate the equivalent current I_e according to formula (16)
7: Predict the SoC according to formula (20)

IV. Model Parameter Identification

In this section, model parameters are identified at different temperature. We used a supercapacitor module MCP0165C0-0048R0SHZ as the test object, which is produced by Supreme Power Solutions Co., Ltd, Beijing, China. The experimental apparatus includes a NEWARE battery test system, a temperature chamber and a PC (Fig. 3). We referred parameter identification in [26] and the test result is as follows. During the capacity test, the cut-off voltage is 29V.

TABLE 1
MODEL PARAMETERS

Temperature(℃)	0	10	20	30
Capacity Q_{max} (A.s)	3244	3306	3308	3290
Internal resistance r_p (mΩ)	4.62	5.80	5.62	5.95
Constant capacitance C_i	141.05	138.37	135.11	138.39
Coefficient K	1.25	1.38	1.5	1.54

Fig. 3. Experimental apparatus

V. Simulations

The prediction algorithm is now evaluated through simulations. We first describe the tools and settings used for evaluation and then demonstrate the accuracy of the predictor.

A. Evaluation Tools and Settings

ADVISOR, originally developed by the National Renewable Energy Laboratory (NREL), allows users to simulate and analyze vehicles, including hybrid electric and fuel cell vehicles. In this software, we applied the aforementioned measured parameters to 100 single supercapacitors and used the supercapacitors as the sole power source in the electric vehicle model VEH_EV1. The vehicle is simulated under a driving cycle: the Economic Commission for Europe + the Extra Urban Driving Cycle (ECE+EUDC).

B. Acquisition of Historical Information

In this section, we aim to extract historical data: historical average power and historical average speed at different SoC. This is because the historical average power can be affected by the initial SoC, since the initial SoC influences the output power capability of supercapacitors [23]. In the software, the output power and speed are equal at the same initial SoC in each simulation. This means that the driving behavior is rather steady and the driver can duplicate the previous trip precisely without changing the speed and route. This is ideal behavior-based driving, and historical average power and historical average speed are unchanged at the same initial SoC in each simulation. In addition, the historical average power and historical average speed are independent of initial SoC in ADVISOR.

C. Simulation Results

The simulation results are achieved by implementing the proposed method under the driving cycle ECE+EUDC (Fig. 4). The simulated SoC is a reference value, which is the final SoC after a complete journey given by ADVISOR. Additionally, the predicted SoC is a prediction value offered by the proposed algorithm before the beginning of the journey.

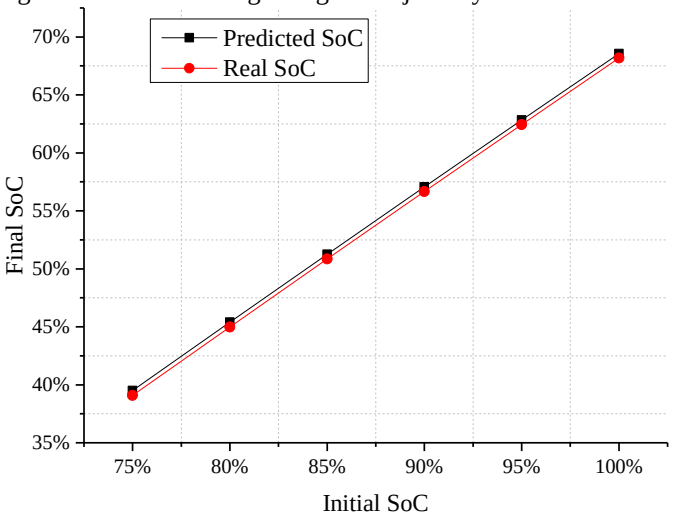

Fig. 4. Prediction results in simulations under ECE+EUDC

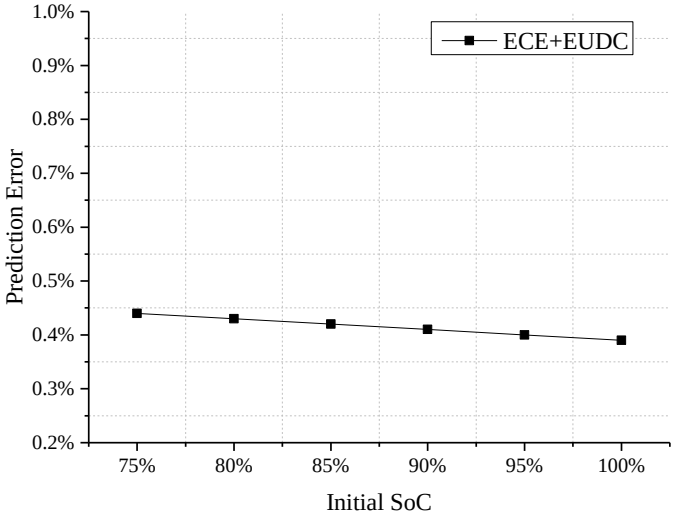

Fig. 5. Prediction errors in the simulations under ECE+EUDC

The prediction results approximate the reference value closely (Fig. 4), although the predicted SoC is slightly larger than the simulated SoC for the driving cycle.

Fig. 5 shows the prediction errors of DBSP under ECE+EUDC in the simulations. The prediction errors are less than 0.5% for the driving cycle, which is an acceptable level of error for the application. The errors are nearly independent of

the initial SoC for the driving cycle because the profiles of the vehicle's speed and average power are the same at the various initial SoC in the simulations, which are ideal values provided by ADVISOR. The small errors imply that driving cycles have nearly no effect on the prediction results.

D. Temperature Influence

Here, we perform the algorithm under different temperature to evaluate the performance. We simulate the process at the initial SoC 75%. The prediction results and prediction error are shown in Fig. 6 and Fig. 7 respectively. From Fig. 6, temperature has weak effects on the real final SoC, since real SoC almost keeps unchanged. In addition, the predicted SoC keeps close to the real SoC at different temperature. In Fig. 7, temperature also has weak effects on the prediction error, since prediction errors almost keep constant at around 0.4%.

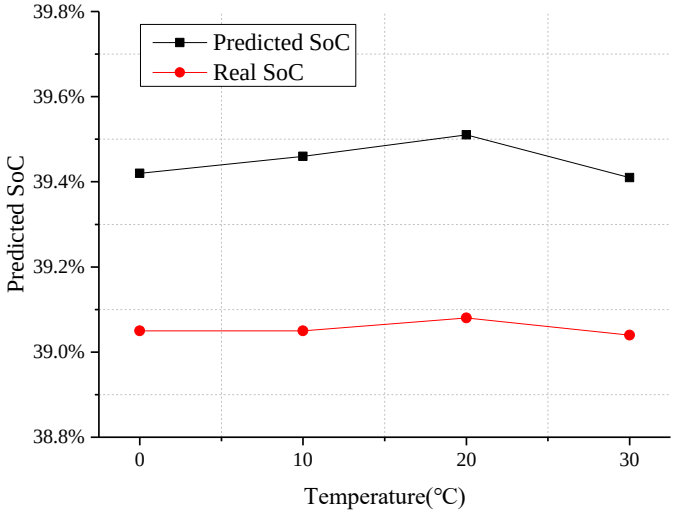

Fig. 6. Prediction results at initial SoC 75% at different temperature

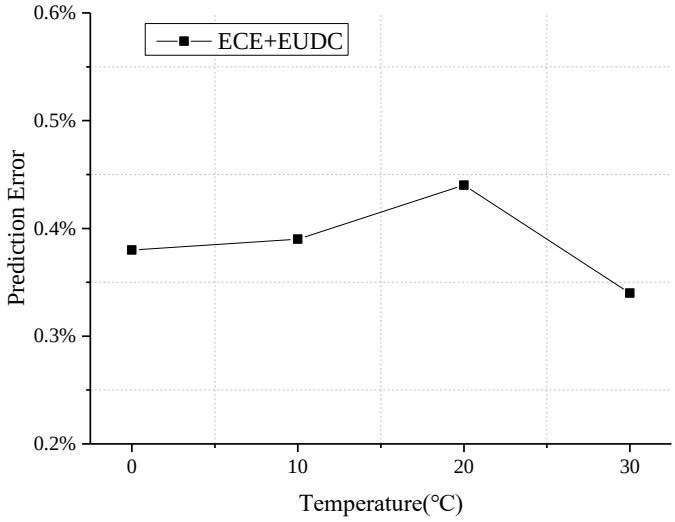

Fig. 7. Prediction errors at different temperature in simulations

VI. Experiments

We now evaluate the proposed SoC predictor experimentally. We first describe the experimental scheme. Then, we use the historical onboard data to test the accuracy of the predictor and perform a qualitative and quantitative analysis.

A. Experimental Scheme

The purpose of the experiments is to simulate drivers driving between a certain departure point and a certain destination. We select a road south of China University of Mining & Technology (CUMT) as the test road. The road incorporates uphill sections, downhill sections, flat roads and bends. In the experiments, one person drives the test vehicle two laps along the planned path (in Fig. 8) from the starting point. The test vehicle is powered by the tested supercapacitor module. During the trips, the terminal voltage, current and speed are recorded by a LabJack T7-PR0 data acquisition card with a sampling frequency of 100 Hz.

Fig. 8. Planned vehicle route

B. Acquisition of Historical Information

The primary historical data is the historical average power. The historical average power is dynamical in practice, which differs from that found in the aforementioned simulations. As each driver's behavior is unique, we obtained the following personal driving behavior profile from experiments conducted with one individual. The historical power profile and historical velocity profile are shown in Figs. 9 and 10, respectively. The historical information is measured in five repeated experiments at each initial SoC point, i.e., 100%, 90%, and 80%. Historical average power values can be determined directly from the data points in Fig. 9. For example, the historical average power with an initial SoC of 95%, can be acquired by interpolation. Data for the historical average speed at different initial SoC can also be obtained in a similar manner from Fig. 10.

The features of the tester's driving behavior in five repeated experiments are as follows, which is unique relative to other driving behaviors. The historical average power is approximately linear with initial SoC. Average power varies at higher initial SoC in five repeated trips . Similarly, historical average speed is roughly linear with initial SoC. Average speed varies greatly with different initial SoC.

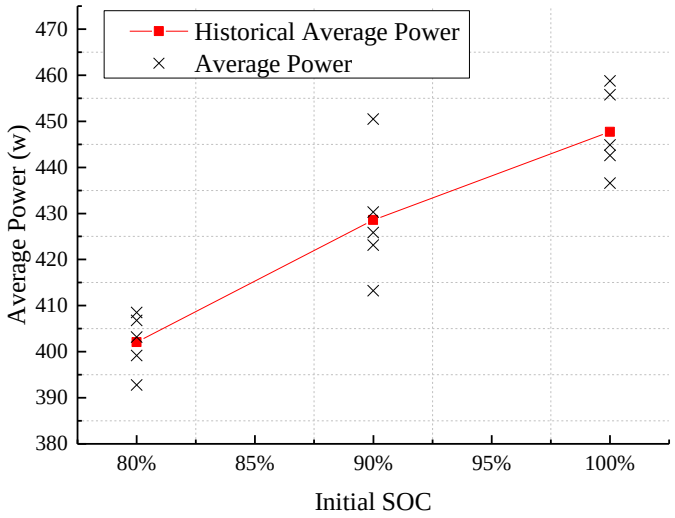

Fig. 9. Historical power profile obtained in five repeated experiments

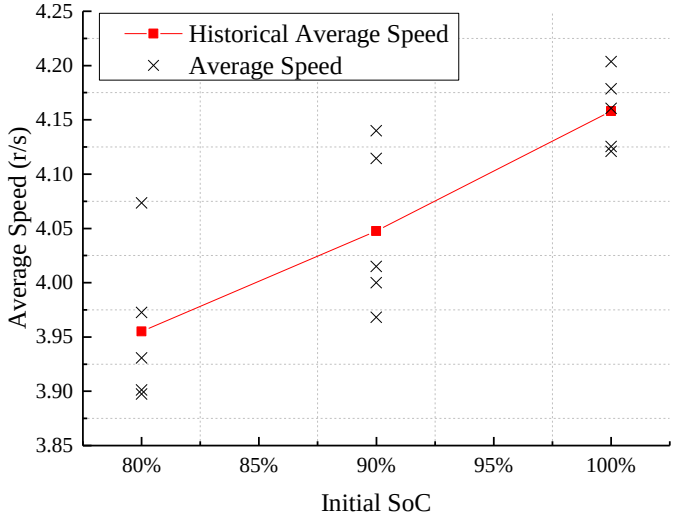

Fig. 10. Historical velocity profile obtained in five repeated experiments

C. *Experimental Results*

Evaluation experiments are conducted at each initial SoC point (100%, 95%, 90%, 85%, 80%, and 75%). The prediction results are acquired in Fig. 11 using the historical information. The results demonstrate that predicted SoC is highly similar to the measured SoC. Generally, the predicted SoC approaches the measured SoC closely. Specially, the predicted SoC at some initial SoC, 85% and 95%, is slightly farther away from the real SoC, compared with other initial SoC. This is because the historical information (average power and average speed) at initial SoC, 85% and 95%, fails to describe the actual average output power and average speed in the verification experiments.

In fact, it is difficult to ensure that the driving parameters (speed and output power) are equal in every experiment, which is different from idealized driving behavior conducted in simulations. Therefore, the total SoC prediction error in experiments includes two parts, a future driving behavior prediction error and an inherent algorithm error which is the accuracy of DBSP itself. The way of calculating the inherent algorithm error is to still use DBSP to predict SoC, but assuming all data including average power, speed and distance in the future driving can be exactly known in advance.

With application of this method, Fig. 12 shows the prediction errors of the proposed algorithm in actual driving experiments on the test road, including the total prediction error and inherent algorithm error. In general, the total prediction error fluctuates within a certain range. The maximum total prediction error is less than 3% at 85% initial SoC and the minimum total prediction error is near zero. By comparison, the inherent algorithm error is steadier and keeps almost unchanged at around 1.2%. This prediction results keeps steady since the influence of historical information is removed and the left is the algorithm error, which reflects the real error of the algorithm. For both curves, the total prediction error is normally larger than the inherent algorithm error except the data point at 100% initial SoC. This is affected by historical information. In detail, history average power can be larger or smaller than that in a real driving situation, which will produce a positive or negative error. This positive or negative error plus the inherent error will change the value of the total prediction error, which explains why the total prediction error is larger or smaller than the inherent error sometimes.

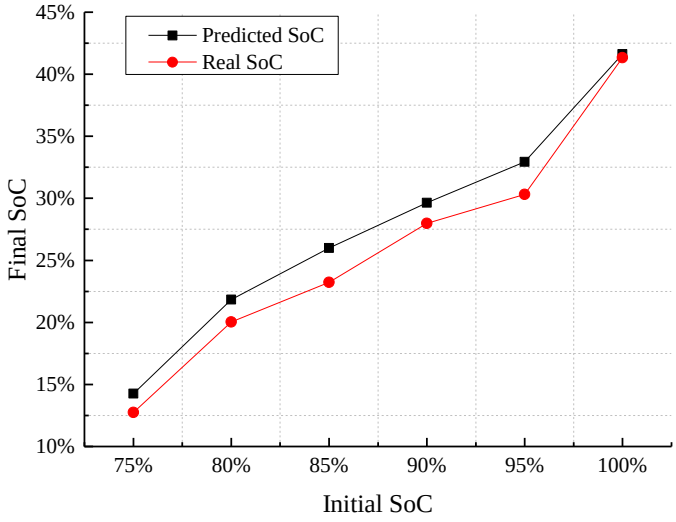

Fig. 11. Predicted SoC and real SoC during experimental trips

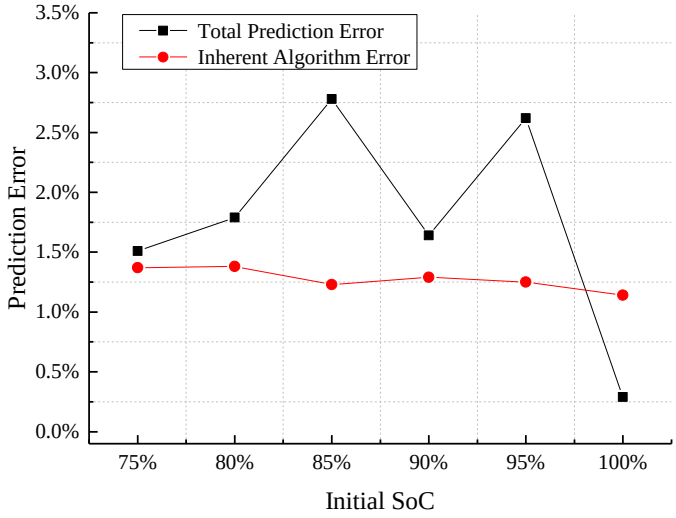

Fig. 12. Prediction errors in experiments

D. *Temperature Influence*

Here, we perform the algorithm at different temperature to evaluate the performance. We use the discharge current obtained from road test as the reference discharge current. These experiments are conducted in the temperature chamber and the battery test system which simulates road driving. We also conducted experiments at 75% initial SoC, and the average power and time is deduced from history data at initial SoC 100%, 90%, 80%. Before showing the results, we need to clarify: the discharge current can only be approximately obtained from but not as exact as the discharge current in the road test. Therefore, final SoC in Fig. 13 is different from the Fig. 11 at the same initial SoC.

The predicted SoC is slightly larger than the real SoC at different temperature, showing a well prediction result (Fig. 13). The total prediction errors are less than 1.6% and fluctuate within a certain range (Fig. 14). The inherent algorithm errors are less than 1.4%. Although there is a slight increase with the temperature, this error is rather small in general.

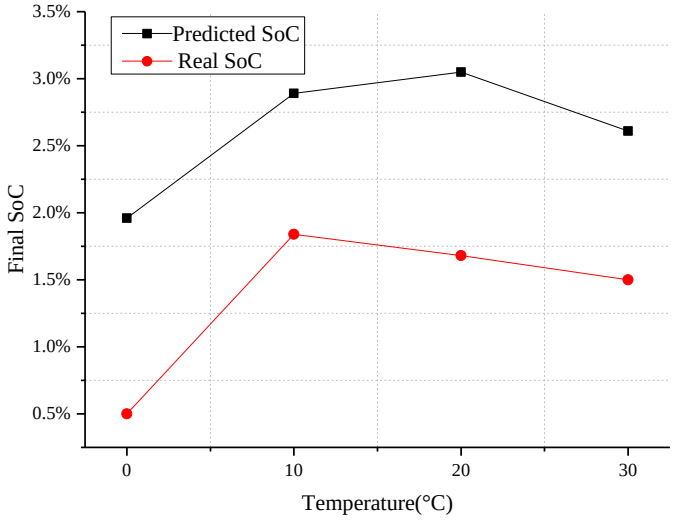

Fig. 13. SoC Prediction results at different temperature in experiments

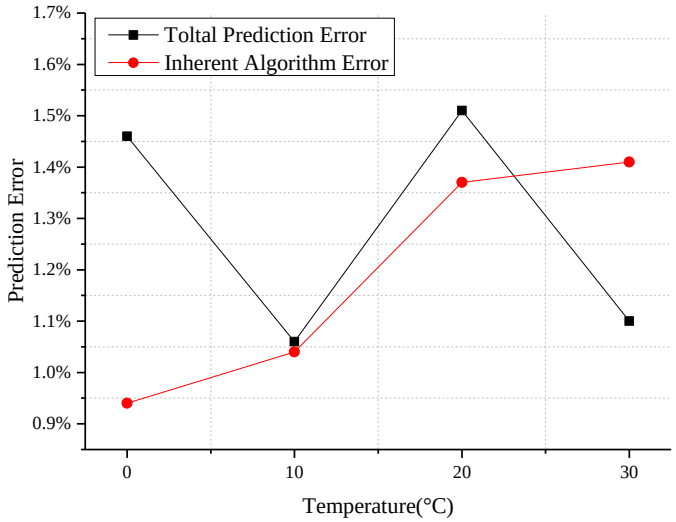

Fig. 14. SoC Prediction error at different temperature in experiments

VII. Conclusions

We have developed an SoC prediction algorithm based on driving behavior to alleviate range anxiety. This paper first establishes two equivalent circuit models of supercapacitors, with one based on the historical average power and the other based on the equivalent current. Second, this paper provides the analytical expression relating the historical average power and predicted SoC. Finally, the DBSP is verified via simulations and experiments at different temperature. The following conclusions can be drawn from the results:

1. The prediction errors are less than 0.5% in simulations, which represent idealized cases. In contrast, the prediction errors are less than 3% in the experiments, which represents practical cases. During these experiments, the inherent algorithm errors are less than 1.5% at different initial SoC and temperature.

2. The SoC prediction can serve as both a qualitative and quantitative analysis, i.e., assessing whether the driver can reach the destination and forecasting what the SoC will be at the end of journey.

Appendix

Current in the Equivalent Circuit of a Supercapacitor Under Constant Discharge

Here, we derive formulas (18) and (19).

The discharge current $I_P(t)$, is dependent on the rate of change of the internal potential $U_c(t)$. We can obtain formula (22) using the relationship between output power P_{ha} and terminal voltage $U_P(t)$. Applying Kirchhoff's Voltage Law to the circuit in Fig. 1 yields formula (21).

$$I_P(t) = -(C_i + KU_c)\frac{dU_c}{dt} \tag{21}$$

$$I_P(t) = \frac{P_{ha}}{U_P(t)} \tag{22}$$

Rearranging (21) and (22) into (23) and then multiplying both sides by the derivative of $U_c(t)$, we obtain the first-order, second-degree differential equation (24).

$$U_c(t) = r_P I_P(t) + U_P(t) \tag{23}$$

$$r_P(C_i + KU_c)\dot{U}_c^2 + U_c\dot{U}_c - \frac{P_{ha}}{C_i + KU_c} = 0 \tag{24}$$

Equation (24) can be written in terms of its two roots λ_1, λ_2, and the full expression can be rewritten as (25), (26).

$$(\dot{U}_c - \lambda_1)(\dot{U}_c - \lambda_2) = 0 \tag{25}$$

$$\lambda_1, \lambda_2 = \frac{-U_c \pm \sqrt{U_c^2 + 4r_p P_{ha}}}{2r_p(C_i + KU_c)} \tag{26}$$

The solution can be obtained after a (U_c, t) variable separation and an integration.

$$t = \frac{C_i}{4P}\left\{\left[U_c(U_c + \sqrt{U_c^2 + 4r_p P_{ha}}) + 4r_p P\ln(U_c + \sqrt{U_c^2 + 4r_p P_{ha}})\right] + \frac{K}{6P}\left[U_c^3 + (U_c^2 + 4r_p P)^{\frac{3}{2}}\right]\right\}_U^{U_{c0}}$$

The expression for the circuit current $I_P(t)$ can now be solved explicitly by substituting (21) for the internal potential

rate of change. The following compact form for supercapacitor current completes the derivation:

$$I_P(t) = -(C_i + KU_c(t))\dot{U}_c(t) = \frac{U_c - \sqrt{U_c^2 + 4r_p P}}{2r_p}$$

REFERENCES

[1] X. Zhang, W. Wang, H. He, L. Hua, and J. Heng, "Optimization of the air-cooled supercapacitor module compartment for an electric bus," *Applied Thermal Engineering*, vol. 112, pp. 1297-1304, 2017.

[2] L. Mir, I. Etxeberriaotadui, I. P. De Arenaza, I. Sarasola, and T. Nieva, "A supercapacitor based light rail vehicle: system design and operations modes," in *energy conversion congress and exposition*, 2009, pp. 1632-1639.

[3] M. Horn, J. MacLeod, M. Liu, J. Webb, and N. Motta, "Supercapacitors: A new source of power for electric cars?," *Economic Analysis and Policy*, 2018.

[4] X. D. Xue, K. W. E. Cheng, R. Raman, S. J. Chan, J. Mei, and C. D. Xu, "Performance Prediction of Light Electric Vehicles Powered by Body-Integrated Super-Capacitors," *2016 International Conference on Electrical Systems for Aircraft, Railway, Ship Propulsion and Road Vehicles & International Transportation Electrification Conference (Esars-Itec)*, 2016.

[5] E. Peralta-Sanchez and J. J. Rodriguez-Rivas, "Electric traction system for a supercapacitor-based electric vehicle," in *Electric Vehicle Symposium and Exhibition*, 2014, pp. 1-6.

[6] Z. Li, C. Zhu, J. Jiang, K. Song, and G. Wei, "A 3-kW Wireless Power Transfer System for Sightseeing Car Supercapacitor Charge," *IEEE Transactions on Power Electronics*, vol. 32, pp. 3301-3316, 2017.

[7] E. Derek Clougherty, E. Lubin Jian, E. Nathan Ball, and C. Derek Wang, "MDR Report: Mellivora, an electric vehicle supercapacitor power supply experiment" (2016). [Online]. Available at http://www.ecs.umass.edu/ece/sdp/sdp16/team19/MDR%20Report%20Team19.pdf (Accessed 27 June 2018).

[8] J.-L. Lu, M.-Y. Yeh, Y.-C. Hsu, S.-N. Yang, C.-H. Gan, and M.-S. Chen, "Operating electric taxi fleets: A new dispatching strategy with charging plans," in *Electric Vehicle Conference (IEVC), 2012 IEEE International*, 2012, pp. 1-8.

[9] J. Neubauer and E. Wood, "The impact of range anxiety and home, workplace, and public charging infrastructure on simulated battery electric vehicle lifetime utility," *Journal of Power Sources*, vol. 257, pp. 12-20, 2014.

[10] D. IEC, "62391-1," *Fixed electric double layer capacitors for use in electronic equipment," Part I: Generic specification (IEC 40/1378/CD: 2003)*, 2004.

[11] L. Shi and M. L. Crow, "Comparison of ultracapacitor electric circuit models," in *power and energy society general meeting*, 2008, pp. 1-6.

[12] C. Wang, H. He, Y. Zhang, and H. Mu, "A comparative study on the applicability of ultracapacitor models for electric vehicles under different temperatures," *Applied Energy*, vol. 196, pp. 268-278, 2017.

[13] N. Devillers, S. Jemei, M. Pera, D. Bienaime, and F. Gustin, "Review of characterization methods for supercapacitor modelling," *Journal of Power Sources*, vol. 246, pp. 596-608, 2014.

[14] W. Vaz, A. K. Nandi, R. G. Landers, and U. O. Koylu, "Electric vehicle range prediction for constant speed trip using multi-objective optimization," *Journal of Power Sources*, vol. 275, pp. 435-446, 2015.

[15] A. Enthaler and F. Gauterin, "Method for Reducing Uncertainties of Predictive Range Estimation Algorithms in Electric Vehicles," in *vehicular technology conference*, 2015, pp. 1-5.

[16] P. OndrúŠKa and I. Posner, "Probabilistic attainability maps: Efficiently predicting driver-specific electric vehicle range," in *Intelligent Vehicles Symposium Proceedings*, 2014, pp. 1169-1174.

[17] G. Dong, J. Wei, Z. Chen, H. Sun, and X. Yu, "Remaining dischargeable time prediction for lithium-ion batteries using unscented Kalman filter," *Journal of Power Sources*, vol. 364, pp. 316-327, 2017.

[18] K. Li, B. H. Soong, and K. J. Tseng, "A high-fidelity hybrid lithium-ion battery model for SOE and runtime prediction," in *Applied Power Electronics Conference and Exposition (APEC), 2017 IEEE*, 2017, pp. 2374-2381.

[19] A. Nadeau, M. Hassanalieragh, G. Sharma, and T. Soyata, "Energy awareness for supercapacitors using Kalman filter state-of-charge tracking," *Journal of Power Sources*, vol. 296, pp. 383-391, 2015.

[20] C.-J. Chiang, J.-L. Yang, and W.-C. Cheng, "Temperature and state-of-charge estimation in ultracapacitors based on extended Kalman filter," *Journal of Power Sources*, vol. 234, pp. 234-243, 2013.

[21] R. German, A. Hammar, R. Lallemand, A. Sari, and P. Venet, "Novel Experimental Identification Method for a Supercapacitor Multipore Model in Order to Monitor the State of Health," *IEEE Transactions on Power Electronics*, vol. 31, pp. 548-559, 2016.

[22] A. E. Mejdoubi, A. Oukaour, H. Chaoui, Y. Slamani, J. Sabor, and H. Gualous, "Online Supercapacitor Diagnosis for Electric Vehicle Applications," *IEEE Transactions on Vehicular Technology*, vol. 65, pp. 4241-4252, 2016.

[23] A. Farmann and D. U. Sauer, "A comprehensive review of on-board State-of-Available-Power prediction techniques for lithium-ion batteries in electric vehicles," *Journal of Power Sources*, vol. 329, pp. 123-137, 2016.

[24] H. Z. Yang and Y. Zhang, "Characterization of supercapacitor models for analyzing supercapacitors connected to constant power elements," *Journal of Power Sources*, vol. 312, pp. 165-171, Apr 30 2016.

[25] X. Chang, D. Lei, S. F. Zhang, S. W. Li, and Y. L. Yang, "Novel Supercapacitor Model Parameter Identification Methods," *Proceedings of 2017 2nd*

International Conference on Power and Renewable Energy (Icpre), pp. 81-86, 2017.

[26] L. Zubieta and R. Bonert, "Characterization of double-layer capacitors for power electronics applications," *Ieee Transactions on Industry Applications*, vol. 36, pp. 199-205, Jan-Feb 2000.

Houlian Wang is currently working toward Ph.D. degree in mechatronic engineering from China University of Mining and Technology, Xuzhou, China. Now, he is also a visiting Ph.D. student with Imperial College London, UK.

His research interests include battery management and low-powered wireless sensor network.

Gongbo Zhou received the B.S. degree in computer science and technology from the Anhui University of Science and Technology, in 2005, and the D.E. degree from the School of Mechanical and Electrical Engineering, China University of Mining and Technology, Xuzhou, China, in 2010.

From 2009 to 2010, he was a visiting Ph.D. student with University of Wisconsin, Madison, WI, USA. He is currently a Professor with the School of Mechatronic Engineering, China University of Mining and Technology. His current research interests include battery management and wireless sensor networks.

Rui Xue received the B.S. degree in vehicle engineering from Anhui Polytechnic University, Wuhu, China, in 2016. He is currently working towards M.S degree in Mechanical Design and Theory from China University of Mining and Technology, Xuzhou, China.

His research direction is wireless sensor network localization and battery energy management.

Yuanjie Lu received B.S. degree in mechatronic engineering from Nanjing University of Technology, Nanjing, China, in 2018. He is currently working towards M.S. degree in mechatronic engineering from China University of Mining and Technology. Xuzhou, China.

His research interests include battery energy management Safety Protection Device for Overwinding and Overfalling.

Julie A McCann is a Full-Professor of Computing Systems at Imperial College London, Department of Computing. Her research centres on highly decentralized and self-organizing scalable algorithms for sensor-based computing systems, wireless networks and energy neurtal computing.

She leads the Adaptive Embedded Systems Engineering Research Group and has worked with Intel, Cisco and NEC etc. on substantive smart city projects. She is an elected peer for the EPSRC and is a Fellow of the BCS.